

Knot data analysis using multiscale Gauss link integral

Li Shen ¹, Hongsong Feng ¹, Fengling Li ², Fengchun Lei ², Jie Wu ³ and Guo-Wei Wei ^{*1,4,5}

¹*Department of Mathematics, Michigan State University, East Lansing, MI 48824, USA*

²*School of Mathematical Sciences, Dalian University of Technology, Dalian 116024, China*

³*Yanqi Lake Beijing Institute of Mathematical Sciences and Applications, 101408, China*

⁴*Department of Biochemistry and Molecular Biology, Michigan State University, MI, 48824, USA*

⁵*Department of Electrical and Computer Engineering, Michigan State University, MI 48824, USA*

Abstract

In the past decade, topological data analysis (TDA) has emerged as a powerful approach in data science. The main technique in TDA is persistent homology, which tracks topological invariants over the filtration of point cloud data using algebraic topology. Although knot theory and related subjects are a focus of study in mathematics, their success in practical applications is quite limited due to the lack of localization and quantization. We address these challenges by introducing knot data analysis (KDA), a new paradigm that incorporating curve segmentation and multiscale analysis into the Gauss link integral. The resulting multiscale Gauss link integral (mGLI) recovers the global topological properties of knots and links at an appropriate scale but offers multiscale feature vectors to capture the local structures and connectivities of each curve segment at various scales. The proposed mGLI significantly outperforms other state-of-the-art methods in benchmark protein flexibility analysis, including earlier persistent homology-based methods. Our approach enables the integration of artificial intelligence (AI) and KDA for general curve-like objects and data.

Key words: Knot data analysis, Gauss link integral, multiscale analysis, protein flexibility.

Contents

1	Introduction	3
2	Methods	4
2.1	Gauss linking integral of open and closed curves	4
2.2	Multiscale Gauss linking integral	5
2.3	Generalized multiscale Gauss linking integral	7
3	Numerical experiment	8
3.1	Protein segmentation and multiscale analysis	8
3.2	Protein flexibility analysis	10
4	Discussions	12
4.1	Absolute multiscale Gauss linking integral	12
4.2	Multiscale featurization	13
4.3	Curve segmentation and multiscale granularity	14

*Corresponding author: weig@msu.edu

5	Conclusion	14
6	Appendix	16

1 Introduction

Knot theory is a branch of mathematics that study mathematical knots [1]. These mathematics knots are often defined as embeddings of a closed circle S^1 into the three-dimensional (3D) Euclidean space. One of the central problems in knot theory is the knot classification problem [2], which asks whether two knots are equivalent or not. Knots that are equivalent can be transformed into each other by a series of continuous deformations, such as stretching or bending the curve, without cutting or gluing any part of it. Such deformations are also known as ambient isotopy [3]. Generally, mathematicians are accustomed to studying a knot in the sense of ambient isotopy as it allows them to focus on the most essential properties of knots themselves rather than on a particular way in which the knot is embedded in the 3D space. Mathematicians have proposed various knot invariants under ambient isotopy which can classify and characterize different type of knots, such as knot crossing number, knot group [1], knot polynomials[2], knot Floer homology [4], Khovanov homology [5], etc.

Knot theory has multiple applications in various fields including physics [6], biochemistry [7], and biology [8, 9, 10]. In the above application scenarios, the studied object does not always meet the ideal state expected mathematically. First of all, such target might not be a closed circle. Secondly, the ambient isotopy may lead to major changes in the properties of the object. For instance, the realization of many application object functions depends on local structural information. An ambient isotopy may completely alter the local structure while keeping the global knot information unchanged. Therefore, it is imperative to develop knot theory-based tools that are robust and effective for data science.

Several attempts have been made to address the aforementioned challenge. Jamroz et al. proposed the protein topology database KnotProt to study knot and slipknot type of proteins [11]. Dabrowski-Tumanski et al.'s Topoly extends the work to include links and spatial graphs, and also enables the calculation of topological polynomials invariant of those structures [12]. Recently, Panagiotou and Kauffman have proposed new invariants for open curves in 3-space [13]. Such method offers a well-defined measurement of entanglement of an open curve. In addition, Baldwin et al. [14] have also made some attempts to localize knot information: intercepting some specific intervals in the linear structure of an open curve gives smaller open curves. Nevertheless, this approach does not really describe local information in 3D space and thus has very limited power in applications related to local functions. In general, current knot and related theories place a major emphasis on preserving global topological properties, and thus, like the classical homology, have very limited success in real-world applications.

We believe that a feasible localization scheme for knot and related theories is to undertake a multiscale analysis. Multiscale analysis has achieved great success in various areas of mathematics, including wavelet theory, differential equations, and topological data analysis (TDA). For example, the key technique in TDA is persistent homology, a mathematical framework that combines concepts from algebraic topology, geometry, and multiscale analysis to analyze complex datasets [15, 16]. It aims to uncover the underlying topological structure and shape of data at different scales, enabling insights that may not be easily discernible with traditional geometric and statistical techniques. By leveraging the power of topological deep learning (TDL) [17], persistent homology offers a unique perspective on understanding the shape and structure of complex datasets, providing valuable insights into the underlying patterns and relationships within the data. TDA has had tremendous success in data science and biological science [18].

The linking number is a numerical topological invariant that measures the extent of linkage between two closed curves in three-dimensional space, representing the number of times that each curve winds around the other. The Gauss linking integral [19], also known as Gauss's integral for the linking number, gives an explicit formulation for the linking number. It is a fundamental tool in the study of knots, links, and other topological structures in three-dimensional space. Gauss linking integral plays an important role in knot theory, algebraic topology, differential geometry, and quantum field theory. For example, for idealized Dirac-string center vortices, the Chern-Simons number can be given by the Gauss link integral [20]. High-order link integrals were proposed [21]. However, these approaches are typically global and qualitative.

The objective of this work is to introduce knot data analysis (KDA) as a new paradigm for data science. To this end, we formulate a new framework called multiscale Gauss linking integral (mGLI) by integrating multiscale analysis with classical knot and knot-related theories. The proposed mGLI can capture both local and global information of knots, curves, and other curve-like objects. Our framework enables us to analyze curve-like objects by applying a specific radius of an open ball around each segment of curve-like objects and provides a metric that describes the degree of local entanglement. As one gradually increases the radius of the open ball, the newly incorporated region within it will reflect its impact on the original structure by altering the value of the metric. When the radius reaches its maximum limit, the metric will retain the global information, such as knots and entangled links. To demonstrate the utility of the proposed mGLI, we apply mGLI to protein flexibility analysis, which successfully constructs a robust correlation between metrics of mGLI and protein B-factors. We show that our KDA tool significantly outperforms other state-of-art methods, including persistent homology, for protein flexibility prediction.

2 Methods

2.1 Gauss linking integral of open and closed curves

Definition 1 (Gauss linking integral). *Given two disjoint open or closed curves l_1 and l_2 , parametrized as $\gamma_1(s)$ and $\gamma_2(t)$, respectively. Then the following double integral gives the the Gauss linking integral that characterizes the degree of interlinking between l_1 and l_2 [22]:*

$$L(l_1, l_2) = \frac{1}{4\pi} \int_{[0,1]} \int_{[0,1]} \frac{\det(\dot{\gamma}_1(s), \dot{\gamma}_2(t), \gamma_1(s) - \gamma_2(t))}{|\gamma_1(s) - \gamma_2(t)|^3} ds dt, \quad (1)$$

where $\dot{\gamma}_1(s)$ and $\dot{\gamma}_2(t)$ are derivative of $\gamma_1(s)$ and $\gamma_2(t)$, respectively.

Proposition 1. *The Gauss linking integral is identical to the average of half the algebraic sum of inter-crossings in the projection of the two curves in any possible projection direction for both open and closed curves.*

Theorem 1 (Panagiotou et al.[13]). *For closed curves, the Gauss linking integral is an integer and a topological invariant. For open curves, the Gauss linking integral is a real number and a continuous function of curve coordinates.*

Definition 2 (Segmentation of Gauss linking integral). *Giving finite curve segments P_n and Q_m for disjoint open or closed curves l_1 and l_2 , respectively, then the segmentation of Gauss linking integral induced by the curve segments is defined as the following $n \times m$ segmentation matrix:*

$$G = \begin{pmatrix} L(p_1, q_1) & L(p_1, q_2) & \cdots & L(p_1, q_m) \\ L(p_2, q_1) & L(p_2, q_2) & \cdots & L(p_2, q_m) \\ \vdots & \vdots & \ddots & \vdots \\ L(p_n, q_1) & L(p_n, q_2) & \cdots & L(p_n, q_m) \end{pmatrix}, \quad (2)$$

where $p_i \in P_n$ and $q_j \in Q_m$ are curve segments of l_1 and l_2 , respectively.

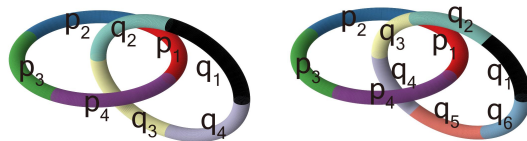


Figure 1: Curve segmentation of the Hopf link.

Theorem 2 (The grand sum of the segmentation matrix). *The grand sum of the segmentation matrix of two curves equals the Gauss linking integral of the original curves:*

$$L(l_1, l_2) = \sum_i \sum_j L(p_i, p_j). \quad (3)$$

Example 1. *Figure 1 shows two different curve segmentation of the Hopf link of two components l_1 and l_2 , with the following parametric equation, respectively:*

$$\gamma_1 = \begin{pmatrix} \cos(2\pi t) \\ \sin(2\pi t) \\ 0 \end{pmatrix} \text{ and } \gamma_2 = \begin{pmatrix} \cos(2\pi s) + 1 \\ 0 \\ \sin(2\pi s) \end{pmatrix}. \quad (4)$$

It is well-known that the Gauss linking integral of the Hopf link shown in Figure 1 equals to -1 . Based on Equation 2, we can obtain the following segmentation of Gauss linking integral:

$$G_1 = \begin{pmatrix} L(p_1, q_1) & L(p_1, q_2) & L(p_1, q_3) & L(p_1, q_4) \\ L(p_2, q_1) & L(p_2, q_2) & L(p_2, q_3) & L(p_2, q_4) \\ L(p_3, q_1) & L(p_3, q_2) & L(p_3, q_3) & L(p_3, q_4) \\ L(p_4, q_1) & L(p_4, q_2) & L(p_4, q_3) & L(p_4, q_4) \end{pmatrix}. \quad (5)$$

We have

$$\begin{aligned} L(p_i, q_j) &= \frac{1}{4\pi} \int_{[\frac{i-1}{4}, \frac{i}{4}]} \int_{[\frac{j-1}{4}, \frac{j}{4}]} \frac{\det(\gamma_1(s), \gamma_2(t), \gamma_1(s) - \gamma_2(t))}{|\gamma_1(s) - \gamma_2(t)|^3} ds dt \\ &= \frac{1}{4\pi} \int_{[\frac{(i-1)\pi}{2}, \frac{i\pi}{2}]} \int_{[\frac{(j-1)\pi}{2}, \frac{j\pi}{2}]} \frac{\cos(\phi) - \cos(\theta) - \cos(\phi)\cos(\theta)}{(3 + 2\cos(\phi) - 2\cos(\theta) - 2\cos(\phi)\cos(\theta))^{\frac{3}{2}}} d\phi d\theta. \end{aligned} \quad (6)$$

Numerical calculations show that

$$G_1 \approx \begin{pmatrix} -0.0640 & -0.1413 & -0.1413 & -0.0640 \\ 0.0193 & -0.0640 & -0.0640 & 0.0193 \\ 0.0193 & -0.0640 & -0.0640 & 0.0193 \\ -0.0640 & -0.1413 & -0.1413 & -0.0640 \end{pmatrix} \quad (7)$$

and the grand sum of G_1 equals -1.000 . Similarly, we have

$$G_2 \approx \begin{pmatrix} -0.0391 & -0.0579 & -0.1083 & -0.1083 & -0.0579 & -0.0391 \\ 0.0137 & 0.0069 & -0.0653 & -0.0653 & 0.0069 & 0.0137 \\ 0.0137 & 0.0069 & -0.0653 & -0.0653 & 0.0069 & 0.0137 \\ -0.0391 & -0.0579 & -0.1083 & -0.1083 & -0.0579 & -0.0391 \end{pmatrix} \quad (8)$$

and the grand sum of G_2 equals -1.000 .

2.2 Multiscale Gauss linking integral

In this section, we introduce the multiscale Gauss linking integral (mGLI) based on the segmentation of the Gauss linking integral. The multiscale Gauss linking integral gives rise to a vectorization of the Gauss linking integral in the multiscale representation, which can be employed as a practical embedding for mathematical measurements in various applications.

Remark 1. *Multiscale analysis requires a definition of distance between objects. Since the objects in the segmentation of Gauss linking integral are curve segments, we need to define the distance of curve segments $d(p_i, q_j)$. Although distance can be defined in various metrics, we choose the Euclidean distance of two points in this study (see more details in Equation 20 and Equation 21). For simplicity, here we simply denote the distance as $d(p_i, q_j)$.*

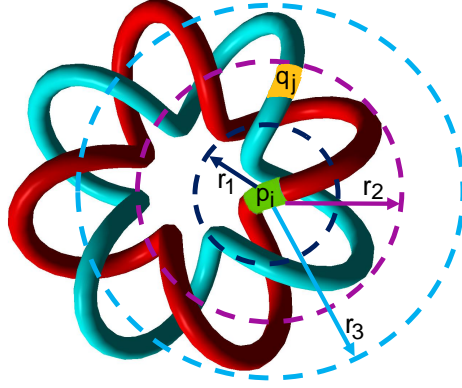


Figure 2: An illustration of multiscale Gauss linking integral with a (2,8) torus link.

Definition 3 (Scaled Gauss linking integral). *Giving a finite set of real numbers $R = \{r_0, r_1, r_2, r_3, \dots, r_k\}$ where $0 = r_0 < r_1 < r_2 < \dots < r_k$, the Gauss linking integral at scale $[r_t, r_{t+1}]$ is defined:*

$$G^{r_t, r_{t+1}} = \begin{pmatrix} \chi_{[r_t, r_{t+1}]}(d(p_1, q_1))L(p_1, q_1) & \chi_{[r_t, r_{t+1}]}(d(p_1, q_2))L(p_1, q_2) & \cdots & \chi_{[r_t, r_{t+1}]}(d(p_1, q_m))L(p_1, q_m) \\ \chi_{[r_t, r_{t+1}]}(d(p_2, q_1))L(p_2, q_1) & \chi_{[r_t, r_{t+1}]}(d(p_2, q_2))L(p_2, q_2) & \cdots & \chi_{[r_t, r_{t+1}]}(d(p_2, q_m))L(p_2, q_m) \\ \vdots & \vdots & \ddots & \vdots \\ \chi_{[r_t, r_{t+1}]}(d(p_n, q_1))L(p_n, q_1) & \chi_{[r_t, r_{t+1}]}(d(p_n, q_2))L(p_n, q_2) & \cdots & \chi_{[r_t, r_{t+1}]}(d(p_n, q_m))L(p_n, q_m) \end{pmatrix}, \quad (9)$$

where

$$\chi_{[r_t, r_{t+1}]}(x) = \begin{cases} 1, & \text{if } x \in [r_t, r_{t+1}] \\ 0, & \text{else} \end{cases} \quad (10)$$

Remark 2. *The scaled Gauss linking integral is used to extract appropriate linking integral within the scale. As shown in Figure 2, we have $G_{ij}^{0, r_1} = 0$, $G_{ij}^{r_1, r_2} = L(p_i, q_j)$, and $G_{ij}^{r_2, r_3} = 0$. By examining multiple Gaussian linking integral at different scales, we obtain an embedding of Gauss linking integral in the multiscale representation.*

Definition 4 (Localized scaled Gauss linking integral). *For given scale $[r_t, r_{t+1}]$, we can define the localized scaled Gauss linking integral at p_i or q_j by the followings:*

$$J^{r_t, r_{t+1}}(p_i) = \sum_{s=1}^m G_{is}^{r_t, r_{t+1}} \quad (11)$$

$$J^{r_t, r_{t+1}}(q_j) = \sum_{s=1}^n G_{sj}^{r_t, r_{t+1}} \quad (12)$$

Remark 3. *The localized scaled Gauss linking integral give rise to a measurement for each curve segment in the curve. By considering different scales, the localized scaled Gauss linking integral provide a featurization of each curve segment u :*

$$Feature(u) = (J^{r_1, r_2}(u), J^{r_2, r_3}(u), \dots, J^{r_{k-1}, r_k}(u)). \quad (13)$$

The resulting feature vectors offer a basis for machine learning, including deep learning, of complex geometric systems.

2.3 Generalized multiscale Gauss linking integral

Vassiliev measure, a generalization of Gauss linking integral, can be applied to open and closed curves in 3-space [23]. Similarly, the proposed mGLI obtained by combining the Gauss linking integral and multiscale process can naturally be applied to links, linkoids, open and closed curves, and other segmentable objects. It can be noticed that any element in the segmentation of the Gauss linking integral is defined on local curve segments. This indicates that one can define a generalized form of the multiscale Gauss linking integral whenever the segmentation of the Gauss linking integral is well-defined on local curve segments. In fact, for any topological or geometric structure that can be segmented into curve segments P_n, Q_m , we can define the following segmentation matrix:

$$\bar{G} = \begin{pmatrix} g(p_1, q_1) & g(p_1, q_2) & \cdots & g(p_1, q_m) \\ g(p_2, q_1) & g(p_2, q_2) & \cdots & g(p_2, q_m) \\ \vdots & \vdots & \ddots & \vdots \\ g(p_n, q_1) & g(p_n, q_2) & \cdots & g(p_n, q_m) \end{pmatrix}, \quad (14)$$

where

$$g(p_i, q_j) = \begin{cases} L(p_i, q_j) & \text{if } p_i \cap q_j \text{ is a null-set,} \\ 0 & \text{else.} \end{cases} \quad (15)$$

In the above definition, unlike in Equation 2, the curve segments in P_n and Q_m are allowed to intersect or

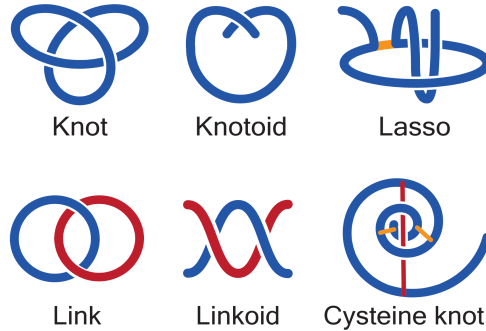


Figure 3: Examples of topological structures which can be studied by multiscale Gauss linking integral. Note that a knotoid is also known as a slipknot [11] in some context.

even be equal. Thus, the mGLI can be applied in multiple topological/geometric structures as long as they can locally be represented as curve segments. These kinds of structures can be commonly found in multiple studies. Here, we present six examples in Figure 3 including knot, knotoid [24], link, linkoid [23], lasso [25], and cysteine knot [26].

Example 2. We exhibits in this example how the segmentation of Gauss linking integral performs on a slipknot shown in Figure 4. Here, we consider a curve segmentation P_7 with itself, giving the following matrix:

$$\bar{G}_1 = \begin{pmatrix} g(p_1, p_1) & g(p_1, p_2) & \cdots & g(p_1, p_7) \\ g(p_2, p_1) & g(p_2, p_2) & \cdots & g(p_2, p_7) \\ \vdots & \vdots & \ddots & \vdots \\ g(p_7, p_1) & g(p_7, p_2) & \cdots & g(p_7, p_7) \end{pmatrix}, \quad (16)$$

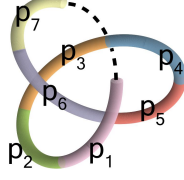


Figure 4: A slipknot with seven curve segments.

Note that $p_i \cap p_j$ is a null-set if and only if $i \neq j$, and thus, we have

$$g(p_i, p_j) = \begin{cases} L(p_i, p_j) & i \neq j \\ 0 & i = j \end{cases}. \quad (17)$$

Then, we have

$$\bar{G}_1 = \begin{pmatrix} 0 & L(p_1, p_2) & \cdots & L(p_1, p_7) \\ L(p_2, p_1) & 0 & \cdots & L(p_2, p_7) \\ \vdots & \vdots & \ddots & \vdots \\ L(p_7, p_1) & L(p_7, p_2) & \cdots & 0 \end{pmatrix}. \quad (18)$$

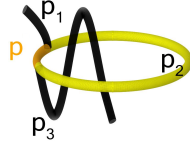


Figure 5: A lasso with four curve segments.

Example 3. In this example, we consider a lasso that has a disulfide bridge (orange p') with a slipknot (black p_1 , yellow p_2 , and black p_3). The segmentation of the Gauss linking integral at this lasso is:

$$\begin{aligned} \bar{G}_2 &= \begin{pmatrix} g(p_1, p_1) & g(p_1, p_2) & g(p_1, p_3) & g(p_1, p') \\ g(p_2, p_1) & g(p_2, p_2) & g(p_2, p_3) & g(p_2, p') \\ g(p_3, p_1) & g(p_3, p_2) & g(p_3, p_3) & g(p_3, p') \\ g(p', p_1) & g(p', p_2) & g(p', p_3) & g(p', p') \end{pmatrix} \\ &= \begin{pmatrix} 0 & g(p_1, p_2) & L(p_1, p_3) & L(p_1, p') \\ L(p_2, p_1) & 0 & L(p_2, p_3) & L(p_2, p') \\ L(p_3, p_1) & L(p_3, p_2) & 0 & L(p_3, p') \\ L(p', p_1) & L(p', p_2) & L(p', p_3) & 0 \end{pmatrix}. \end{aligned} \quad (19)$$

3 Numerical experiment

3.1 Protein segmentation and multiscale analysis

In this section, we assess the effectiveness of the proposed generalized mGLI in predicting protein B-factors. Protein B-factors, also known as temperature factors or atomic displacement parameters, provide information about the mobility and flexibility of atoms in a protein structure. B-factors are derived from crystallographic experiments or other experimental means and are represented as a numerical value associated with each atom in the protein. High B-factors indicate increased atomic mobility, suggesting regions of the protein that are flexible or undergoing conformational changes. Low B-factors, on the other hand, indicate rigid regions with limited atomic motion.

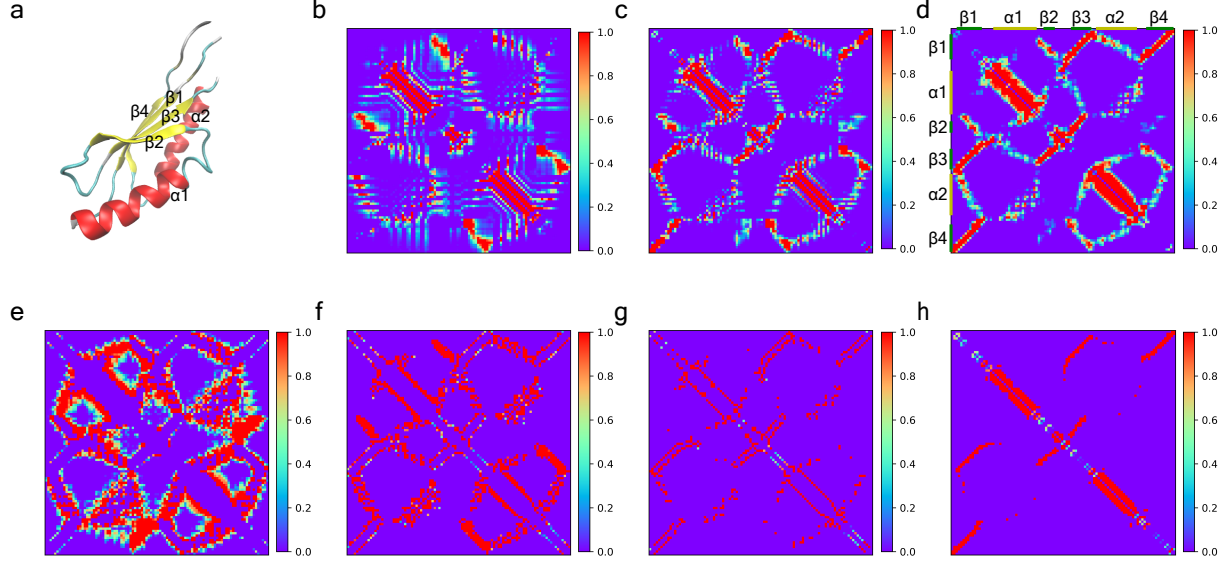


Figure 6: An illustration of multiscale Gauss linking integral on a protein (PDBID: 1J27). **a** The 3D structure of 1J27 consisting of two α -helices and four β -sheets. **b** The segmentation of the Gauss linking integral of protein 1J27. **c** The absolute value of Gauss linking integral matrix of protein 1J27. **d** The absolute Gauss linking integral matrix of protein 1J27. **e-h** Absolute Gauss linking integral matrices of protein 1J27 at different scales.

To predict protein B-factors, we consider a protein as an open curve, acknowledging that the polypeptide chain of a protein molecule can be seen as an open polygon l whose vertices are corresponding to the C_α atoms, while the edges represent the pseudobonds that connect a C_α atom to another one in an adjacent amino acid residue.

Here, we propose a curve segmentation induced by C_α atoms:

$$p_i = \{x \in l_1 | f(x, c_i) = \inf_{c \in C} f(x, c)\}, 1 \leq i \leq n, \quad (20)$$

where $f(a, b)$ is the distance of points a and b along l , and C is the set of C_α atoms. Then, the $d(p_i, q_j)$ assumed in 1 can be defined:

$$d(p_i, q_j) = d_E(c_i, c_j), \quad (21)$$

where d_E is the Euclidean distance in the 3D space.

Then, the segmentation of Gauss linking integral that investigates the inter-crossings between segments of the protein can be given:

$$G = \begin{pmatrix} \hat{L}(p_1, p_1) & \hat{L}(p_1, p_2) & \cdots & \hat{L}(p_1, p_n) \\ \hat{L}(p_2, p_1) & \hat{L}(p_2, p_2) & \cdots & \hat{L}(p_2, p_n) \\ \vdots & \vdots & \ddots & \vdots \\ \hat{L}(p_n, p_1) & \hat{L}(p_n, p_2) & \cdots & \hat{L}(p_n, p_n) \end{pmatrix} = \begin{pmatrix} 0 & L(p_1, p_2) & \cdots & L(p_1, p_n) \\ L(p_2, p_1) & 0 & \cdots & L(p_2, p_n) \\ \vdots & \vdots & \ddots & \vdots \\ L(p_n, p_1) & L(p_n, p_2) & \cdots & 0 \end{pmatrix}. \quad (22)$$

Here, we present the illustration of Gauss linking integral matrix for a protein (PDBID: 1J27) in Figure 6b. This matrix can reflect much structural information about the protein. Therefore, the Gauss linking integral matrix itself is an excellent structural featurization method for proteins.

Also, it is worth noting that the value of Gauss linking integral is subject to its consideration of the curve orientations. On a specific task that does not depend on the orientation of the curve, removing the influence of the orientation may give a better results. In particular, in protein B-factor analysis, the effects of two differently oriented structures on a certain C_α atom will hardly cancel each other out. In fact, by taking the absolute value of segmentation of Gauss linking integral, the orientation information can be greatly reduced.

As shown in [Figure 6c](#), a large number of interlaced patterns are removed. Further, to completely ignore orientation information, we consider the absolute Gauss linking integral

$$\bar{L}(l_1, l_2) = \frac{1}{4\pi} \int_{[0,1]} \int_{[0,1]} \left| \frac{\det(\dot{\gamma}_1(s), \dot{\gamma}_2(t), \gamma_1(s) - \gamma_2(t))}{|\gamma_1(s) - \gamma_2(t)|^3} \right| ds dt, \quad (23)$$

with its corresponding matrix. An illustration of this approach is given in [Figure 6d](#).

To present featurization of the absolute Gauss linking integral, we consider the localized scaled absolute Gauss linking integral at each curve segment around each C_α atom of various scales, generating a multiscale Gauss linking integral feature vector. We validate in numerous protein structures that there exists a high correlation coefficients between the reciprocal of featurization of segments ([Equation 13](#)) and the corresponding C_α atom’s B-factor.

3.2 Protein flexibility analysis

Protein flexibility analysis is the study of the dynamic behavior and conformational changes of proteins. Proteins are not rigid structures but rather exhibit flexibility and undergo various motions and deformations essential for their biological functions. Protein flexibility analysis involves investigating the conformational space accessible to a protein, understanding its inherent flexibility, and exploring how it relates to protein function, stability, and interactions with other molecules. It provides insights into how proteins can adopt different shapes and conformations to perform their roles, such as enzyme catalysis, molecular recognition, and signal transduction.

Several computational methods have been proposed for protein flexibility analysis. The Gauss network model (GNM) [27] and anisotropic network model (ANM) [28], and normal mode analysis (NMA)[29] have been widely used for their simplicity. However, Park et al. [30] have demonstrated that both GNM and NMA were ineffective in analyzing numerous protein structures. Their findings revealed that, on average, the correlation coefficient of GNM and NMA, for the three protein sets, categorized as small-size, medium-size, and large-size, was below 0.6 and 0.5, respectively. Recently, many advanced methods have been proposed for this problem, including flexibility rigidity index-based methods, pFFRI [31] and opFFRI [31] and topology-based methods, including atom-specific persistent homology (ASPH) [32] and evolutionary homology (EH) [33].

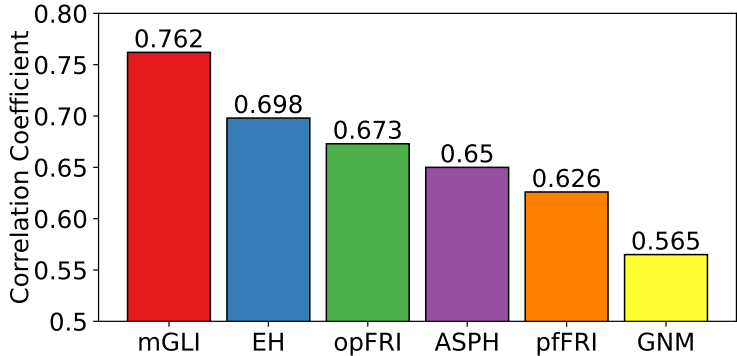


Figure 7: Comparison of B-factor predictions by six methods for 364 proteins.

To assess the performance of the proposed multiscale Gauss linking integral (mGLI) for protein flexibility analysis, we utilized a benchmark dataset comprising 364 protein structures sourced from [31]. This dataset was used for comparisons against previous methods, namely opFFRI [31], pFFRI [31], and GNM [30]. In our evaluation, we set the mGLI with a maximal cutoff of 27Å.

In [Figure 7](#), we present the comparative results of mGLI with previous methods for each protein in the dataset (refer to [Table 2](#) for detailed information). Remarkably, mGLI outperformed the previous methods

in 320 out of 364 proteins. On average, mGLI achieved the highest correlation coefficient of 0.762, surpassing the values of 0.674 for opFRI, 0.628 for pfFRI, and 0.567 for GNM. This represents an improvement of 13.1%, 21.3%, and 34.4% respectively. These results strongly suggest that mGLI is a promising method for protein flexibility analysis, as the higher correlation coefficients obtained indicate its effectiveness.

Protein set	EH[33]	ASPH[32]	opFRI[31]	pfFRI[31]	GNM[30]	NMA[30]	mGLI
Small	0.773	0.870	0.667	0.594	0.541	0.480	0.933
Medium	0.729	0.680	0.664	0.605	0.550	0.482	0.813
Large	0.665	0.610	0.636	0.591	0.529	0.494	0.750

Table 1: Average correlation coefficients for C_α B-factor prediction of our mGLI method with previous EH, opFRI, pfFRI, GNM, and NMA for three protein sets of different size.

In addition, to validate the effectiveness of mGLI for predicting C_α atom B-factors in proteins of different sizes, we compared our method with previous approaches including EH [33], ASPH [32], opFRI [31], pfFRI [31], GNM [30], and NMA [30] on three protein sets, as shown in Table 1.

mGLI achieved average correlation coefficients of 0.933, 0.813, and 0.750 for the small, medium, and large protein sets, respectively, in predicting C_α atom B-factors. Our results on the three datasets significantly outperformed the previous methods, demonstrating improvements of 27.3%, 11.5%, and 12.7% on the small, medium, and large protein sets, respectively, compared to the previous state-of-the-art method EH.

The improvement of our method in predicting protein B-factors is primarily attributed to the clever utilization of knot theory. Traditional B-factor analysis methods primarily focus on individual atoms and their spatial positions in three-dimensional space, considering the thermal motion and disorder of atoms within a protein structure. However, the consideration of bonding interactions between atoms, which indirectly influences the observed B-factor values, is rarely utilized in B-factor analysis. By incorporating knot theory, our method introduces the concept of pseudobonds between protein atoms, thereby capturing the influence of bonding interactions.

The combination of knot theory with the multiscale procedure allows for the localization of measurements provided by the knot theory, taking advantage of the spatial positions and environments of atoms. This synergy between multiscale analysis and knot theory results in a powerful method for protein B-factor prediction, highlighting the potential of multiscale approaches in localizing measurements derived from knot theory.

To provide a direct visualization of the multiscale Gauss linking integral (mGLI), we consider an example using a probable antibiotics synthesis protein (PDBID: 1V70) with a residue number of 105, as shown in Figure 8. Traditional GNM methods exhibit a large error around residues 1-10. In contrast, mGLI successfully predicts the B-factor of this region. The predictions of mGLI are directly obtained from the multiscale Gauss linking integral features. A visualization of the multiscale Gauss linking integral features has been displayed in the bottom right of Figure 8. For each scale, we consider the accumulated absolute Gauss linking integral. A bar corresponding to the color and the accumulated value is placed below it. Note that we label all value exceed a specific value as red (3.0 in this case). Thus we could notice that the upper bound of scale required to accumulate the absolute Gauss linking integral value of each C_α atom to 3.0 is different. In general, the smaller the upper limit of scale needed to reach a specific value, the smaller the corresponding B-factor value. In fact, the peaks in the blue and green areas at the bottom often coincide with the peaks of the experimental B-factor.

The above observations are quite general. We can further validate these findings by providing another visualization using a monomeric cyan fluorescent protein (PDBID: 2HQK), as shown in Figure 9. In this visualization, we label all absolute Gauss linking integral values exceed 4.0 as red. The protein 2HQK has a residue number of 219, which is more than twice that of 1V70. As expected, there are more peaks in its B-factors. Interestingly, each peak in the B-factor plot corresponds nicely to a peak in the visualization of the absolute Gauss linking integral feature. This correlation reinforces the relationship between the B-factor

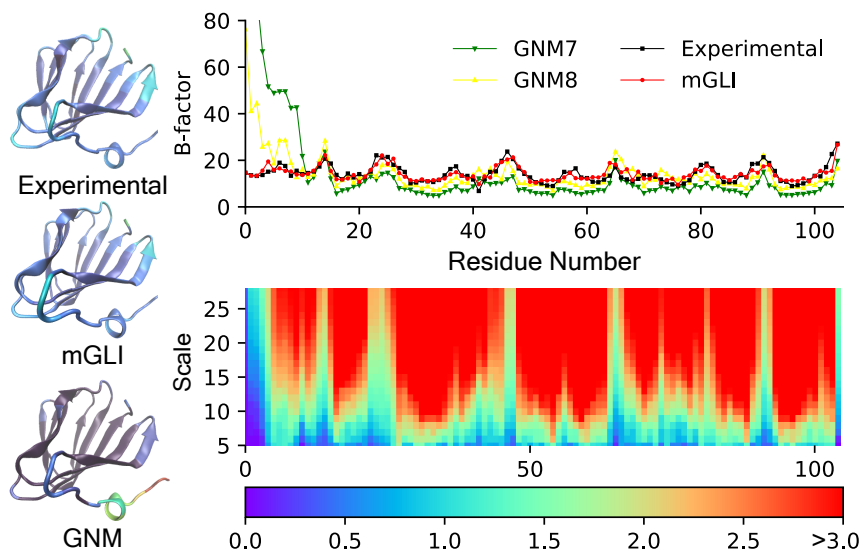


Figure 8: The visualization of mGLI method on the probable antibiotics synthesis protein 1V70. **Left** are the 3D structures of 1V70, colored by experimental B-factor, mGLI predicted B-factor, and GNM predicted B-factor, from top to bottom, respectively. **Right top** is the comparison of GNM7, GNM8, and mGLI prediction values and experimental value for each residue. The x -axis represents the residue number, and the y -axis represents the B-factor. **Right bottom** is the vitalization of mGLI features with the maximal cutoff at 30\AA . The x -axis represents the residue number and the y -axis represents the supreme of filtration range. Note that all value exceed 3.0 are labeled as red. GNM7 represents the GNM with cutoff distance 7\AA .

values and the absolute Gauss linking integral. Furthermore, the absolute Gauss linking integral feature demonstrates how mGLI avoids the erroneous predictions made by traditional GNM methods in the area around residues 50-60. This showcases the advantage of mGLI in accurately capturing the protein’s flexibility and providing more reliable predictions. By examining these different protein examples, we consistently observe the correlation between the absolute Gauss linking integral feature and the experimental B-factor values, highlighting the effectiveness of mGLI in protein B-factor prediction.

4 Discussions

4.1 Absolute multiscale Gauss linking integral

The Gauss linking integral provides information that previous methods cannot capture, which is one of the key factors contributing to the success of mGLI. To illustrate the information contained in mGLI, we compare the segmentation of the absolute multiscale Gauss linking integral with the previous transient probability matrix (TPM) [34] for protein 1J27. The structural information that can be observed through the previous method becomes more evident and clear in mGLI. For example, in the TPM, the $\alpha 1$ - $\alpha 1$ and $\alpha 2$ - $\alpha 2$ interactions are represented as slightly thicker yellow blocks along the diagonal. In contrast, in mGLI, these interactions are depicted as more expressive and prominent large red blocks. This enhanced visualization allows for a better distinction of the self-interaction of the alpha chain from other structural elements, such as the self-interaction of the region between $\beta 2$ and $\beta 3$. Moreover, the contrast between different values within each block is stronger in mGLI compared to TPM. This is particularly evident in the blocks representing interactions such as $\alpha 1$ - $\alpha 2$, $\beta 1$ - $\alpha 2$, $\beta 1$ - $\beta 2$, and so on. In the multiscale analysis, the differences in mGLI values at different scales are further amplified, providing insights into varying structural information. Overall, mGLI offers a more expressive and informative representation of the protein structure compared to the previous TPM method, enabling a better understanding of the intricate interactions within the protein.

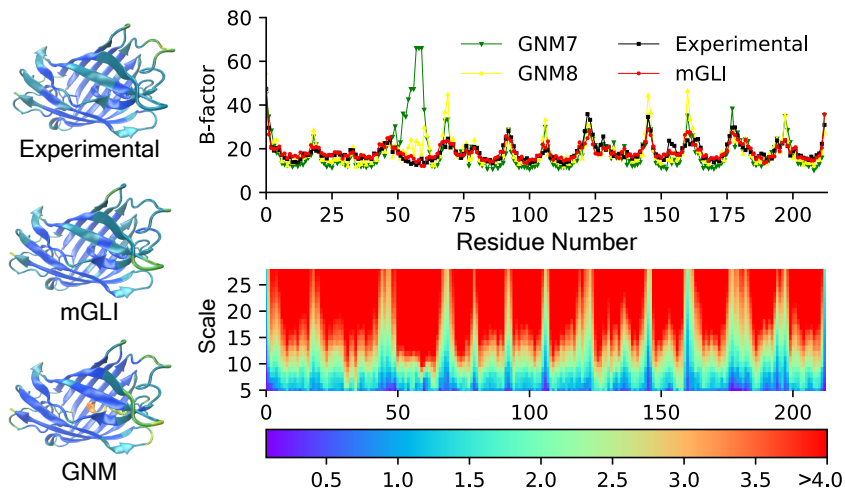


Figure 9: The visualization of mGLI method on the monomeric cyan fluorescent protein 2HQK. **Left** are the 3D structures of 2HQK, colored by experimental B-factor, mGLI predicted B-factor, and GNM predicted B-factor, from top to bottom, respectively. **Right top** is the comparison of GNM7, GNM8, and mGLI prediction value and experimental value for each residue. The x -axis represents the residue number, and the y -axis represents the B-factor. **Right bottom** is the virtualization of mGLI features with the maximal cutoff at 30\AA . The x -axis represents the residue number and the y -axis represents the supreme of scales. Note that all values exceed 4.0 are labeled as red. GNM7 represents the GNM with cutoff distance 7\AA .

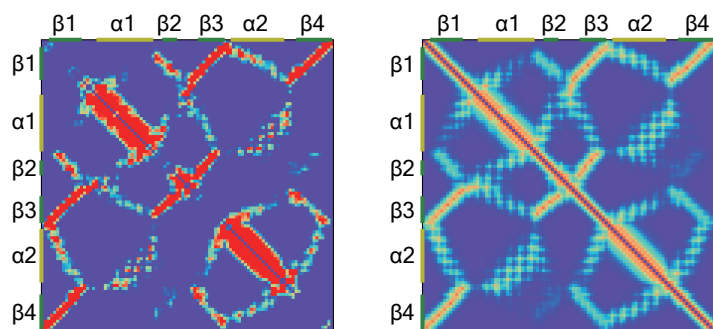


Figure 10: **Left** is the absolute Gauss linking integral matrix for protein 1J27. **Right** is the transient probability matrix (TPM) for protein 1J27 [34]. Each point in top and left are colored green or yellow, if the point represents a residue that is in a β -sheet or an α -helix of 1J27.

4.2 Multiscale featurization

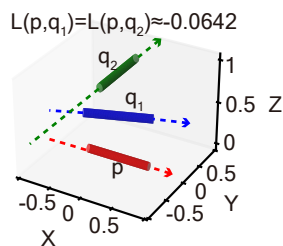


Figure 11: An example of line segments in different scales reporting the same Gauss linking integral.

The process of multiscale vectorizing Gauss linking integral in the multiscale analysis allows mGLI to extract a wealth of information directly related to the spatial arrangement of segments. Each scale captures the Gauss linking integral at a different level of granularity, enabling the discrimination of various segment arrangements.

For example, [Figure 11](#) illustrates two different segment arrangements of q in 3-dimensional space that have identical Gauss linking integrals with p (i.e., $L(p, q_1) = L(p, q_2)$). Without the multiscale process, it would be challenging to differentiate between these arrangements based on the Gauss linking integral alone. However, by considering different scales such as $[0, 0.5]$ and $[0.5, 1]$, the arrangements can be distinguished.

4.3 Curve segmentation and multiscale granularity

In principle, our method allows for the arbitrary combination of curve segmentations with any multiscale schemes. However, in practical applications, the performance of mGLI is highly dependent on the selection of curve segmentations and multiscale schemes. First and foremost, the values of the Gauss linking integral of a local curve segment depend not only on their spatial alignment but also on their relative lengths compared to the global curve. When the length of a curve segment approaches zero, the corresponding Gauss linking integral approximates to 0. Similarly, as the curve segments expand to cover the global curve, the Gauss linking integral returns global information. In both cases, the Gauss linking integral fails to extract useful spatial information regarding local alignments. Secondly, the selection of the multiscale scheme impacts the featurization of the Gauss linking integral. Ideally, different scales should capture different spatial structure information. If the information difference between scales is too small, it can result in a large number of identical or trivial features. Conversely, if the difference is too large, it may lead to the loss of details.

In the specific context of our protein flexibility analysis, we naturally choose a segment that precisely covers a single C_α atom along the polymer chain. Additionally, in our study, the multiscale scheme is selected to start from 5Å and extend up to 27Å, with each scale interval set at 1Å. This choice is based on the fact that the average distance between C_α atoms is approximately 3.8Å. Such a selection of the multiscale scheme results in a powerful featurization method that provides abundant representations of local protein structures.

5 Conclusion

In recent years, topological data analysis (TDA) has experienced rapid growth across various scientific and engineering disciplines. The central technique of TDA, persistent homology, utilizes a multiscale filtration process to enrich algebraic topology. However, the impact of knot theory and related mathematical approaches on data science has been limited, partly due to their global formalism.

This work introduces knot data analysis (KDA) as a powerful new paradigm for data science. Our approach involves partitioning knots and other curved objects into segments and conducting a multiscale analysis at each segment. At each scale, multiscale Gauss link integrals (mGLIs) are defined to capture the local structure and connectivity. These mGLIs allow for the measurement of the properties of knots and links at different scales, ultimately recovering their global properties at a sufficiently large scale. Additionally, we extend mGLIs to encompass various segmentable objects, such as knots, knotoids, lassos, links, linkoids, cysteine knots, and more.

While persistent homology remains a global technique despite filtration, our proposed KDA offers a local approach that focuses on delineating the localized environment around each segment at different scales. By adopting this localized perspective, KDA provides valuable insights into the specific characteristics and relationships within the data.

To showcase the effectiveness of the proposed KDA, we apply the multiscale Gauss link integral (mGLI) to protein flexibility prediction. By utilizing mGLI, we can quantify the relationship between C_α atoms at different scales, enabling a comprehensive analysis of protein flexibility.

In our study, we conducted experiments using four benchmark datasets and compared the performance of mGLI with several previous methods, including a persistent homology-based approach. The results of these extensive experiments consistently demonstrate the superiority of mGLI. Specifically, mGLI achieves a minimum improvement of 13% compared to the previous state-of-the-art methods. Notably, it outperforms the persistent homology-based method by approximately 21%.

These results highlight the significant potential of the proposed KDA in the field of data science. By leveraging the power of mGLI and its ability to capture multiscale relationships, KDA offers promising opportunities for improving various data analysis tasks.

Since mGLI offers multiscale representations of a wide range of spatial structure and connectivity information, it can be leveraged by machine learning algorithms, enabling artificial intelligence to extract powerful and effective insights into segmentable structures. The rich information captured by mGLI allows machine learning algorithms to explore and understand the intricate relationships and patterns within the data. This enables AI systems to make more accurate predictions, classify complex structures, and uncover hidden features that may not be apparent through traditional approaches.

Acknowledgment

This work was supported in part by NIH grants R01GM126189, R01AI164266, and R35GM148196 , NSF grants DMS-2052983, DMS-1761320, DMS-2245903, and IIS-1900473, NASA grant 80NSSC21M0023, MSU Foundation, Bristol-Myers Squibb 65109, and Pfizer.

6 Appendix

In this appendix, detailed B-factor predictions for a set of 364 proteins are presented. Comparison is given to opFRI[31], pfFRI[31], GNM[30], and mGLI.

PDBID	N	opFRI[31]	pfFRI[31]	GNM[30]	mGLI	PDBID	N	opFRI	pfFRI	GNM	mGLI
1ABA	87	0.727	0.698	0.613	0.856	1PEF	18	0.888	0.826	0.808	1.0
1AHO	64	0.698	0.625	0.562	0.788	1PEN	16	0.516	0.465	0.27	0.858
1AIE	31	0.588	0.416	0.155	0.985	1PMY	123	0.671	0.654	0.685	0.763
1AKG	16	0.373	0.35	0.185	0.854	1PZ4	114	0.828	0.781	0.843	0.925
1ATG	231	0.613	0.578	0.497	0.743	1Q9B	43	0.746	0.726	0.656	0.985
1BGF	124	0.603	0.539	0.543	0.921	1QAU	112	0.678	0.672	0.62	0.731
1BX7	51	0.726	0.623	0.706	0.893	1QKI	3912	0.809	0.751	0.645	0.678
1BYI	224	0.543	0.491	0.552	0.678	1QTO	122	0.543	0.52	0.334	0.725
1CCR	111	0.58	0.512	0.351	0.643	1R29	122	0.65	0.631	0.556	0.781
1CYO	88	0.751	0.702	0.741	0.91	1R7J	90	0.789	0.621	0.368	0.929
1DF4	57	0.912	0.889	0.832	0.975	1RJU	36	0.517	0.447	0.431	0.839
1E5K	188	0.746	0.732	0.859	0.831	1RRO	112	0.435	0.372	0.529	0.691
1ES5	260	0.653	0.638	0.677	0.681	1SAU	114	0.742	0.671	0.596	0.837
1ETL	12	0.71	0.609	0.628	1.0	1TGR	104	0.72	0.711	0.714	0.805
1ETM	12	0.544	0.393	0.432	0.97	1TZV	141	0.837	0.82	0.841	0.915
1ETN	12	0.089	0.023	-0.274	0.67	1U06	55	0.474	0.429	0.434	0.893
1EW4	106	0.65	0.644	0.547	0.797	1U7I	267	0.778	0.762	0.691	0.758
1F8R	1932	0.878	0.859	0.738	0.746	1U9C	221	0.6	0.577	0.522	0.754
1FF4	65	0.718	0.613	0.674	0.871	1UHA	83	0.726	0.665	0.638	0.863
1FK5	93	0.59	0.568	0.485	0.779	1UKU	102	0.665	0.661	0.742	0.847
1GCO	1044	0.766	0.693	0.646	0.706	1ULR	87	0.639	0.594	0.495	0.822
1GK7	39	0.845	0.773	0.821	0.935	1UOY	64	0.713	0.653	0.671	0.877
1GVD	52	0.781	0.732	0.591	0.933	1USE	40	0.438	0.146	-0.142	0.964
1GXU	88	0.748	0.634	0.421	0.882	1USM	77	0.832	0.809	0.798	0.964
1H6V	2927	0.488	0.429	0.306	0.504	1UTG	70	0.691	0.61	0.538	0.849
1HJE	13	0.811	0.686	0.616	0.975	1V05	96	0.629	0.599	0.632	0.742
1I71	83	0.549	0.516	0.549	0.691	1V70	105	0.622	0.492	0.162	0.794
1IDP	441	0.735	0.715	0.69	0.729	1VRZ	21	0.792	0.695	0.677	0.999
1IFR	113	0.697	0.689	0.637	0.77	1W2L	97	0.691	0.564	0.397	0.845
1K8U	89	0.553	0.531	0.378	0.763	1WBE	204	0.591	0.577	0.549	0.706
1KMM	1499	0.749	0.744	0.558	0.727	1WHI	122	0.601	0.539	0.27	0.591
1KNG	144	0.547	0.536	0.512	0.723	1WLY	322	0.695	0.679	0.666	0.701
1KR4	110	0.635	0.612	0.466	0.693	1WPA	107	0.634	0.577	0.417	0.793
1KYC	15	0.796	0.763	0.754	1.0	1X3O	80	0.6	0.559	0.654	0.72
1LR7	73	0.679	0.657	0.62	0.882	1XY1	18	0.832	0.645	0.447	1.0
1MF7	194	0.687	0.681	0.7	0.717	1XY2	8	0.619	0.57	0.562	1.0
1N7E	95	0.651	0.609	0.497	0.794	1Y6X	87	0.596	0.524	0.366	0.739
1NKD	59	0.75	0.703	0.631	0.913	1YJO	6	0.375	0.333	0.434	1.0
1NKO	122	0.619	0.535	0.368	0.703	1YZM	46	0.842	0.834	0.901	0.975
1NLS	238	0.669	0.53	0.523	0.777	1Z21	96	0.662	0.638	0.433	0.739
1NNX	93	0.795	0.789	0.631	0.903	1ZCE	146	0.808	0.757	0.77	0.911
1NOA	113	0.622	0.604	0.615	0.629	1ZVA	75	0.756	0.579	0.69	0.934

PDBID	N	opFRI	pfFRI	GNM	mGLI	PDBID	N	opFRI	pfFRI	GNM	mGLI
1NOT	13	0.746	0.622	0.523	0.999	2A50	457	0.564	0.524	0.281	0.527
1O06	20	0.91	0.874	0.844	1.0	2AGK	233	0.705	0.694	0.512	0.753
1O08	221	0.562	0.333	0.309	0.8	2AH1	939	0.684	0.593	0.521	0.557
1OB4	16	0.776	0.763	0.75	1.0	2B0A	186	0.639	0.603	0.467	0.664
1OB7	16	0.737	0.545	0.652	1.0	2BCM	413	0.555	0.551	0.477	0.442
1OPD	85	0.555	0.409	0.398	0.689	2BF9	36	0.606	0.554	0.68	0.999
1P9I	29	0.754	0.742	0.625	0.975	2BRF	100	0.795	0.764	0.71	0.857
2CE0	99	0.706	0.598	0.529	0.85	2C71	205	0.658	0.649	0.56	0.848
2CG7	90	0.551	0.539	0.379	0.743	2OLX	4	0.917	0.888	0.885	1.0
2COV	534	0.846	0.823	0.812	0.638	2PKT	93	0.162	0.003	0.193	0.641
2CWS	227	0.647	0.64	0.696	0.773	2PLT	99	0.508	0.484	0.509	0.663
2D5W	1214	0.689	0.682	0.681	0.648	2PMR	76	0.693	0.682	0.619	0.878
2DKO	253	0.816	0.812	0.69	0.789	2POF	440	0.682	0.651	0.589	0.637
2DPL	565	0.596	0.538	0.658	0.479	2PPN	107	0.677	0.638	0.668	0.765
2DSX	52	0.337	0.333	0.127	0.65	2PSF	608	0.526	0.5	0.565	0.552
2E10	439	0.798	0.796	0.692	0.777	2PTH	193	0.822	0.784	0.767	0.837
2E3H	81	0.692	0.682	0.605	0.722	2Q4N	153	0.711	0.667	0.74	0.79
2EAQ	89	0.753	0.69	0.695	0.862	2Q52	412	0.756	0.748	0.621	0.71
2EHP	248	0.804	0.804	0.773	0.762	2QJL	99	0.594	0.584	0.594	0.812
2EHS	75	0.72	0.713	0.747	0.851	2R16	176	0.582	0.495	0.618	0.675
2ERW	53	0.461	0.253	0.199	0.858	2R6Q	138	0.603	0.54	0.529	0.653
2ETX	389	0.58	0.556	0.632	0.621	2RB8	93	0.727	0.614	0.517	0.808
2FB6	116	0.791	0.786	0.74	0.838	2RE2	238	0.652	0.613	0.673	0.683
2FG1	157	0.62	0.617	0.584	0.741	2RFR	154	0.693	0.671	0.753	0.816
2FN9	560	0.607	0.595	0.611	0.659	2V9V	135	0.555	0.548	0.528	0.679
2FQ3	85	0.719	0.692	0.348	0.868	2VE8	515	0.744	0.643	0.616	0.569
2G69	99	0.622	0.59	0.436	0.812	2VH7	94	0.775	0.726	0.596	0.897
2G7O	68	0.785	0.784	0.66	0.952	2VIM	104	0.413	0.393	0.212	0.598
2G7S	190	0.67	0.644	0.649	0.76	2VPA	204	0.763	0.755	0.576	0.641
2GKG	122	0.688	0.646	0.711	0.859	2VQ4	106	0.68	0.679	0.555	0.861
2GOM	121	0.586	0.584	0.491	0.461	2VY8	149	0.77	0.724	0.533	0.701
2GXG	140	0.847	0.78	0.52	0.9	2VYO	210	0.675	0.648	0.729	0.767
2GZQ	191	0.505	0.382	0.369	0.86	2W1V	548	0.68	0.68	0.571	0.66
2HQK	213	0.824	0.809	0.365	0.89	2W2A	350	0.706	0.638	0.589	0.631
2HYK	238	0.585	0.575	0.51	0.626	2W6A	117	0.823	0.748	0.647	0.761
2I24	113	0.593	0.498	0.494	0.711	2WJ5	96	0.484	0.44	0.357	0.656
2I49	398	0.714	0.683	0.601	0.739	2WUJ	100	0.739	0.598	0.598	0.668
2IBL	108	0.629	0.625	0.352	0.723	2WW7	150	0.499	0.471	0.356	0.46
2IGD	61	0.585	0.481	0.386	0.825	2WWE	111	0.692	0.582	0.628	0.807
2IMF	203	0.652	0.625	0.514	0.719	2X1Q	240	0.534	0.478	0.443	0.549
2IP6	87	0.654	0.578	0.572	0.862	2X25	168	0.632	0.598	0.403	0.793
2IVY	88	0.544	0.483	0.271	0.838	2X3M	166	0.744	0.717	0.655	0.832
2J32	244	0.863	0.848	0.855	0.802	2X5Y	171	0.718	0.705	0.694	0.811
2J9W	200	0.716	0.705	0.662	0.745	2X9Z	262	0.583	0.578	0.574	0.64
2JKU	35	0.805	0.695	0.656	0.993	2XHF	310	0.606	0.591	0.569	0.721
2JLI	100	0.779	0.613	0.622	0.836	2Y0T	101	0.778	0.774	0.798	0.835

PDBID	N	opFRI	pfFRI	GNM	mGLI	PDBID	N	opFRI	pfFRI	GNM	mGLI
2JLJ	115	0.741	0.72	0.527	0.844	2Y72	170	0.78	0.754	0.766	0.874
2MCM	113	0.789	0.713	0.639	0.846	2Y7L	319	0.928	0.797	0.747	0.742
2NLS	36	0.605	0.559	0.53	0.942	2Y9F	149	0.771	0.762	0.664	0.835
2NR7	194	0.803	0.785	0.727	0.868	2YLB	400	0.807	0.807	0.675	0.7
2NUH	104	0.835	0.691	0.771	0.908	2YNY	315	0.813	0.804	0.706	0.427
2O6X	306	0.814	0.799	0.651	0.797	2ZCM	357	0.458	0.422	0.42	0.434
2OA2	132	0.571	0.456	0.458	0.794	2ZU1	360	0.689	0.672	0.653	0.649
2OCT	192	0.567	0.55	0.54	0.675	3A0M	148	0.807	0.712	0.392	0.704
2OHW	256	0.614	0.539	0.475	0.74	3A7L	128	0.713	0.663	0.756	0.733
2OKT	342	0.433	0.411	0.336	0.517	3AMC	614	0.675	0.669	0.581	0.726
2OL9	6	0.909	0.904	0.689	1.0	3AUB	116	0.614	0.608	0.637	0.674
3BA1	312	0.661	0.624	0.621	0.687	3B5O	230	0.644	0.629	0.601	0.614
3BED	261	0.845	0.82	0.684	0.769	3MD4	12	0.86	0.781	0.914	1.0
3BQX	139	0.634	0.481	0.297	0.72	3MD5	12	0.649	0.413	-0.218	1.0
3BZQ	99	0.532	0.516	0.466	0.717	3MEA	166	0.669	0.669	0.6	0.694
3BZZ	100	0.485	0.45	0.6	0.616	3MGN	348	0.205	0.119	0.193	0.267
3DRF	547	0.559	0.549	0.488	0.601	3MRE	383	0.661	0.641	0.567	0.513
3DWV	325	0.707	0.661	0.547	0.702	3N11	325	0.614	0.583	0.517	0.608
3E5T	228	0.502	0.489	0.296	0.601	3NE0	208	0.706	0.645	0.659	0.811
3E7R	40	0.706	0.687	0.642	0.929	3NGG	94	0.696	0.689	0.719	0.847
3EUR	140	0.431	0.427	0.577	0.52	3NPV	495	0.702	0.653	0.677	0.574
3F2Z	149	0.824	0.792	0.74	0.861	3NVG	6	0.721	0.617	0.597	1.0
3F7E	254	0.812	0.803	0.811	0.809	3NZL	73	0.627	0.583	0.506	0.891
3FCN	158	0.64	0.606	0.632	0.847	3O0P	194	0.727	0.706	0.734	0.772
3FE7	91	0.583	0.533	0.276	0.685	3O5P	128	0.734	0.698	0.63	0.902
3FKE	250	0.525	0.476	0.435	0.769	3OBQ	150	0.649	0.645	0.655	0.647
3FMY	66	0.701	0.655	0.556	0.876	3OQY	234	0.698	0.686	0.637	0.725
3FOD	48	0.532	0.44	-0.126	0.768	3P6J	125	0.774	0.767	0.81	0.893
3FSO	221	0.831	0.817	0.793	0.6	3PD7	188	0.77	0.723	0.589	0.778
3FTD	240	0.722	0.713	0.634	0.733	3PES	165	0.697	0.642	0.683	0.686
3FVA	6	0.835	0.825	0.789	1.0	3PID	387	0.537	0.531	0.642	0.575
3G1S	418	0.771	0.7	0.63	0.653	3PIW	154	0.758	0.744	0.717	0.861
3GBW	161	0.82	0.747	0.51	0.839	3PKV	221	0.625	0.597	0.568	0.673
3GHJ	116	0.732	0.511	0.196	0.813	3PSM	94	0.876	0.79	0.745	0.74
3HFO	197	0.691	0.67	0.518	0.646	3PTL	289	0.543	0.541	0.468	0.535
3HHP	1234	0.72	0.716	0.683	0.643	3PVE	347	0.718	0.667	0.568	0.581
3HNY	156	0.793	0.723	0.758	0.89	3PZ9	357	0.709	0.709	0.678	0.803
3HP4	183	0.534	0.5	0.573	0.677	3PZZ	12	0.945	0.922	0.95	1.0
3HWU	144	0.754	0.748	0.841	0.861	3Q2X	6	0.922	0.904	0.866	1.0
3HYD	7	0.966	0.95	0.867	1.0	3Q6L	131	0.622	0.577	0.605	0.699
3HZ8	192	0.617	0.502	0.475	0.634	3QDS	284	0.78	0.745	0.568	0.742
3I2V	124	0.486	0.441	0.301	0.562	3QPA	197	0.587	0.442	0.503	0.866
3I2Z	138	0.613	0.599	0.317	0.597	3R6D	221	0.688	0.669	0.495	0.774
3I4O	135	0.735	0.714	0.738	0.732	3R87	132	0.452	0.419	0.286	0.701
3I7M	134	0.667	0.635	0.695	0.774	3RQ9	162	0.51	0.403	0.242	0.507
3IHS	169	0.586	0.565	0.409	0.583	3RY0	128	0.616	0.606	0.47	0.77

PDBID	N	opFRI	pfFRI	GNM	mGLI	PDBID	N	opFRI	pfFRI	GNM	mGLI
3IVV	149	0.817	0.797	0.693	0.734	3RZY	139	0.8	0.784	0.849	0.879
3K6Y	227	0.586	0.535	0.301	0.629	3S0A	119	0.562	0.524	0.526	0.672
3KBE	140	0.705	0.704	0.611	0.726	3SD2	86	0.523	0.421	0.237	0.734
3K GK	190	0.784	0.775	0.68	0.662	3SEB	238	0.801	0.712	0.826	0.871
3KZD	85	0.647	0.611	0.475	0.719	3SED	124	0.709	0.658	0.712	0.82
3L41	220	0.718	0.716	0.669	0.678	3SO6	150	0.675	0.666	0.63	0.848
3LAA	169	0.827	0.647	0.659	0.82	3SR3	637	0.619	0.611	0.624	0.67
3LAX	106	0.734	0.73	0.584	0.898	3SUK	248	0.644	0.633	0.567	0.619
3LG3	833	0.658	0.614	0.589	0.652	3SZH	697	0.817	0.815	0.697	0.706
3LJI	272	0.612	0.608	0.551	0.619	3T0H	208	0.808	0.775	0.694	0.889
3M3P	249	0.584	0.554	0.338	0.757	3T3K	122	0.796	0.748	0.735	0.918
3M8J	178	0.73	0.728	0.628	0.674	3T47	141	0.592	0.527	0.447	0.649
3M9J	210	0.639	0.574	0.296	0.499	3TDN	357	0.458	0.419	0.24	0.584
3M9Q	176	0.591	0.51	0.471	0.627	3TOW	152	0.578	0.556	0.571	0.802
3MAB	173	0.664	0.591	0.451	0.589	3TUA	210	0.665	0.658	0.588	0.815
3U6G	248	0.635	0.632	0.526	0.527	3TYS	75	0.853	0.8	0.791	0.939
3U97	77	0.753	0.736	0.712	0.916	4DT4	160	0.776	0.738	0.716	0.813
3UCI	72	0.589	0.526	0.495	0.844	4EK3	287	0.68	0.68	0.674	0.676
3UR8	637	0.666	0.652	0.597	0.651	4ERY	318	0.74	0.701	0.688	0.78
3US6	148	0.698	0.586	0.553	0.878	4ES1	95	0.648	0.625	0.551	0.813
3V1A	48	0.531	0.487	0.583	0.978	4EUG	225	0.57	0.529	0.405	0.617
3V75	285	0.604	0.596	0.491	0.71	4F01	448	0.633	0.372	0.688	0.377
3VN0	193	0.84	0.837	0.812	0.734	4F3J	143	0.617	0.598	0.551	0.7
3VOR	182	0.602	0.557	0.484	0.674	4FR9	141	0.671	0.655	0.501	0.807
3VUB	101	0.625	0.61	0.607	0.84	4G14	15	0.467	0.323	0.356	1.0
3VVV	108	0.833	0.741	0.753	0.899	4G2E	151	0.76	0.755	0.758	0.863
3VZ9	163	0.785	0.749	0.695	0.725	4G5X	550	0.786	0.754	0.743	0.775
3W4Q	773	0.737	0.725	0.649	0.628	4G6C	658	0.591	0.59	0.528	0.501
3ZBD	213	0.651	0.516	0.632	0.776	4G7X	194	0.688	0.587	0.624	0.622
3ZIT	152	0.43	0.404	0.392	0.412	4GA2	144	0.528	0.485	0.406	0.642
3ZRX	221	0.59	0.562	0.391	0.501	4GMQ	92	0.678	0.628	0.55	0.862
3ZSL	138	0.691	0.687	0.526	0.87	4GS3	90	0.544	0.522	0.547	0.778
3ZZP	74	0.524	0.46	0.448	0.944	4H4J	236	0.81	0.806	0.689	0.832
3ZZY	226	0.746	0.709	0.728	0.621	4H89	168	0.682	0.588	0.596	0.672
4A02	166	0.618	0.516	0.303	0.748	4HDE	168	0.745	0.728	0.615	0.911
4ACJ	167	0.748	0.746	0.759	0.752	4HJP	281	0.703	0.649	0.51	0.764
4AE7	186	0.724	0.717	0.717	0.717	4HWM	117	0.638	0.622	0.499	0.767
4AM1	345	0.674	0.619	0.46	0.665	4IL7	85	0.446	0.404	0.316	0.635
4ANN	176	0.551	0.536	0.47	0.641	4J11	357	0.62	0.562	0.401	0.528
4AVR	188	0.68	0.605	0.65	0.784	4J5O	220	0.793	0.757	0.777	0.824
4AXY	54	0.7	0.623	0.72	0.696	4J5Q	146	0.742	0.742	0.689	0.787
4B6G	558	0.765	0.756	0.669	0.758	4J78	305	0.658	0.648	0.608	0.574
4B9G	292	0.844	0.816	0.763	0.832	4JG2	185	0.746	0.736	0.543	0.775
4DD5	387	0.615	0.596	0.351	0.712	4JVU	207	0.723	0.697	0.553	0.697
4DKN	423	0.781	0.761	0.539	0.728	4JYP	534	0.688	0.682	0.538	0.711
4DND	95	0.763	0.75	0.582	0.623	4KEF	133	0.58	0.53	0.324	0.701

PDBID	N	opFRI	pfFRI	GNM	mGLI	PDBID	N	opFRI	pfFRI	GNM	mGLI
4DPZ	109	0.73	0.726	0.651	0.795	5CYT	103	0.441	0.421	0.331	0.7
4DQ7	328	0.69	0.683	0.376	0.763	6RXN	45	0.614	0.574	0.594	0.825

Table 2: The comparison of correlation coefficient of mGLI with previous methods including opFRI, prFRI, and GNM. N refers to the number of residues in the protein. And the best value for each protein is marked in bold.

References

- [1] Richard H Crowell and Ralph Hartzler Fox. *Introduction to knot theory*, volume 57. Springer Science & Business Media, 2012.
- [2] Colin C Adams. *The knot book*. American Mathematical Soc., 1994.
- [3] Mark Anthony Armstrong. *Basic topology*. Springer Science & Business Media, 2013.
- [4] Ciprian Manolescu. An introduction to knot floer homology. *Physics and mathematics of link homology*, 680:99–135, 2014.
- [5] Mikhail Khovanov. A categorification of the jones polynomial. 2000.
- [6] Tomotada Ohtsuki. *Quantum invariants: A study of knots, 3-manifolds, and their sets*, volume 29. World Scientific, 2002.
- [7] Chengzhi Liang and Kurt Mislow. Knots in proteins. *Journal of the American Chemical Society*, 116(24):11189–11190, 1994.
- [8] DW Summers. The role of knot theory in dna research. In *Geometry and Topology*, pages 297–318. CRC Press, 2020.
- [9] Tamar Schlick, Qiyao Zhu, Abhishek Dey, Swati Jain, Shuting Yan, and Alain Laederach. To knot or not to knot: multiple conformations of the sars-cov-2 frameshifting rna element. *Journal of the American Chemical Society*, 143(30):11404–11422, 2021.
- [10] Kenneth C Millett, Eric J Rawdon, Andrzej Stasiak, and Joanna I Sulowska. Identifying knots in proteins. *Biochemical Society Transactions*, 41(2):533–537, 2013.
- [11] Michal Jamroz, Wanda Niemyska, Eric J Rawdon, Andrzej Stasiak, Kenneth C Millett, Piotr Sulkowski, and Joanna I Sulowska. Knotprot: a database of proteins with knots and slipknots. *Nucleic acids research*, 43(D1):D306–D314, 2015.
- [12] Pawel Dabrowski-Tumanski, Pawel Rubach, Wanda Niemyska, Bartosz Ambrozy Gren, and Joanna Ida Sulowska. Topoly: Python package to analyze topology of polymers. *Briefings in Bioinformatics*, 22(3):bbaa196, 2021.
- [13] Eleni Panagiotou and Louis H Kauffman. Knot polynomials of open and closed curves. *Proceedings of the Royal Society A*, 476(2240):20200124, 2020.
- [14] Quenisha Baldwin, Bobby Sumpter, and Eleni Panagiotou. The local topological free energy of the sars-cov-2 spike protein. *Polymers*, 14(15):3014, 2022.
- [15] Herbert Edelsbrunner, John Harer, et al. Persistent homology-a survey. *Contemporary mathematics*, 453(26):257–282, 2008.
- [16] Afra Zomorodian and Gunnar Carlsson. Computing persistent homology. In *Proceedings of the twentieth annual symposium on Computational geometry*, pages 347–356, 2004.

- [17] Zixuan Cang and Guo-Wei Wei. Topologynet: Topology based deep convolutional and multi-task neural networks for biomolecular property predictions. *PLoS computational biology*, 13(7):e1005690, 2017.
- [18] Jiahui Chen, Yuchi Qiu, Rui Wang, and Guo-Wei Wei. Persistent laplacian projected omicron ba. 4 and ba. 5 to become new dominating variants. *Computers in Biology and Medicine*, 151:106262, 2022.
- [19] Carl Friedrich Gauss. Integral formula for linking number. In *Zur mathematischen theorie der electro-dynamische wirkungen*, 5:605, 1833.
- [20] John M Cornwall and Noah Graham. Sphalerons, knots, and dynamical compactification in yang-mills-chern-simons theories. *Physical Review D*, 66(6):065012, 2002.
- [21] Mitchell A Berger. Third-order link integrals. *Journal of Physics A: Mathematical and General*, 23(13):2787, 1990.
- [22] Renzo L Ricca and Bernardo Nipoti. Gauss’linking number revisited. *Journal of Knot Theory and Its Ramifications*, 20(10):1325–1343, 2011.
- [23] Eleni Panagiotou and Louis H Kauffman. Vassiliev measures of complexity of open and closed curves in 3-space. *Proceedings of the Royal Society A*, 477(2254):20210440, 2021.
- [24] Neslihan Gügümcü and Louis H Kauffman. New invariants of knotoids. *European Journal of Combinatorics*, 65:186–229, 2017.
- [25] Wanda Niemyska, Pawel Dabrowski-Tumanski, Michal Kadlof, Ellinor Haglund, Piotr Sulkowski, and Joanna I Sulkowska. Complex lasso: new entangled motifs in proteins. *Scientific reports*, 6(1):36895, 2016.
- [26] Pawel Dabrowski-Tumanski, Pawel Rubach, Dimos Goundaroulis, Julien Dorier, Piotr Sulkowski, Kenneth C Millett, Eric J Rawdon, Andrzej Stasiak, and Joanna I Sulkowska. Knotprot 2.0: a database of proteins with knots and other entangled structures. *Nucleic acids research*, 47(D1):D367–D375, 2019.
- [27] AJ Rader, Chakra Chennubhotla, Lee-Wei Yang, and Ivet Bahar. The gaussian network model: Theory and applications. In *Normal mode analysis*, pages 65–88. Chapman and Hall/CRC, 2005.
- [28] Eran Eyal, Lee-Wei Yang, and Ivet Bahar. Anisotropic network model: systematic evaluation and a new web interface. *Bioinformatics*, 22(21):2619–2627, 2006.
- [29] Ivet Bahar and AJ Rader. Coarse-grained normal mode analysis in structural biology. *Current opinion in structural biology*, 15(5):586–592, 2005.
- [30] Jun-Koo Park, Robert Jernigan, and Zhijun Wu. Coarse grained normal mode analysis vs. refined gaussian network model for protein residue-level structural fluctuations. *Bulletin of mathematical biology*, 75:124–160, 2013.
- [31] Kristopher Opron, Kelin Xia, and Guo-Wei Wei. Fast and anisotropic flexibility-rigidity index for protein flexibility and fluctuation analysis. *The Journal of chemical physics*, 140(23):06B617_1, 2014.
- [32] David Bramer and Guo-Wei Wei. Atom-specific persistent homology and its application to protein flexibility analysis. *Computational and mathematical biophysics*, 8(1):1–35, 2020.
- [33] Zixuan Cang, Elizabeth Munch, and Guo-Wei Wei. Evolutionary homology on coupled dynamical systems with applications to protein flexibility analysis. *Journal of applied and computational topology*, 4:481–507, 2020.
- [34] Kristopher Opron, Kelin Xia, and Guo-Wei Wei. Communication: Capturing protein multiscale thermal fluctuations. *The Journal of chemical physics*, 142(21):06B401_1, 2015.